

**REPORT DOCUMENTATION PAGE**

Form Approved  
OMB No. 0704-0188

The public reporting burden for this collection of information is estimated to average 1 hour per response, including the time for reviewing instructions, searching existing data sources, gathering and maintaining the data needed, and completing and reviewing the collection of information. Send comments regarding this burden estimate or any other aspect of this collection of information, including suggestions for reducing the burden, to the Department of Defense, Executive Services and Communications Directorate (0704-0188). Respondents should be aware that notwithstanding any other provision of law, no person shall be subject to any penalty for failing to comply with a collection of information if it does not display a currently valid OMB control number.

**PLEASE DO NOT RETURN YOUR FORM TO THE ABOVE ORGANIZATION.**

1. REPORT DATE (DD-MM-YYYY) 10-02-2012	2. REPORT TYPE Journal Article	3. DATES COVERED (From - To)
---	-----------------------------------	------------------------------

4. TITLE AND SUBTITLE Current and Density Observations of Packets of Nonlinear Internal Waves on the Outer New Jersey Shelf	5a. CONTRACT NUMBER
	5b. GRANT NUMBER
	5c. PROGRAM ELEMENT NUMBER 0602435N

6. AUTHOR(S) William Teague, Hemantha Wijesekera, W. Avera, Z.R. Hallock	5d. PROJECT NUMBER
	5e. TASK NUMBER
	5f. WORK UNIT NUMBER 73-6248-B0-5

7. PERFORMING ORGANIZATION NAME(S) AND ADDRESS(ES) Naval Research Laboratory Oceanography Division Stennis Space Center, MS 39529-5004	8. PERFORMING ORGANIZATION REPORT NUMBER NRL/JA/7330-10-0407
---	---

9. SPONSORING/MONITORING AGENCY NAME(S) AND ADDRESS(ES) Office of Naval Research One Liberty Center 875 North Randolph Street, Suite 1425 Arlington, VA 22203-1995	10. SPONSOR/MONITOR'S ACRONYM(S) ONR
	11. SPONSOR/MONITOR'S REPORT NUMBER(S)

12. DISTRIBUTION/AVAILABILITY STATEMENT  
Approved for public release, distribution is unlimited.

20120217 366

13. SUPPLEMENTARY NOTES

14. ABSTRACT  
Closely spaced observations of nonlinear internal waves (NLIWs) were made on the outer continental shelf off New Jersey in June 2009. Nearly full water column measurements of current velocity were made with four acoustic Doppler current profilers (ADCPs) that were moored about 5 km apart on the bottom along a line approximately normal to the bathymetry between water depths of 67 and 92 m. Density profiles were obtained from two vertical strings of temperature and conductivity sensors that were deployed near each of the interior ADCP moorings. In addition, a towed ScanFish provided profiles and fixed-level records of temperature and salinity through several NLIW packets near the moorings. Several case studies were selected to describe the propagation of the NLIWs. One to three solitary waves of depression were observed in five selected packets. There were also occurrences of multiple-phase dispersive wave packets. The average propagation speed corrected for advection of the observed waves was  $0.51 \pm 0.09 \text{ m s}^{-1}$ . The waves were directed primarily shoreward (~northwestward) along the mooring line with average wavelengths and periods of about 300 m and 10 min, respectively. Wave amplitudes and energies decreased with decreasing water depth. The observed wave parameters can be locally described by a two-layer Korteweg -de Vries (KdV) model, except for the decreasing amplitudes, which may be due to shear-induced dissipation and/or bottom drag. The various complementary observations utilized in this study present a unique description of NLIWs.

15. SUBJECT TERMS  
density currents, internal waves, continental shelf

16. SECURITY CLASSIFICATION OF:			17. LIMITATION OF ABSTRACT UU	18. NUMBER OF PAGES 15	19a. NAME OF RESPONSIBLE PERSON William J. Teague
a. REPORT Unclassified	b. ABSTRACT Unclassified	c. THIS PAGE Unclassified			19b. TELEPHONE NUMBER (Include area code) 228-688-4734

## Current and Density Observations of Packets of Nonlinear Internal Waves on the Outer New Jersey Shelf

W. J. TEAGUE, H. W. WIJESEKERA, AND W. E. AVERA

*Naval Research Laboratory, Stennis Space Center, Mississippi*

Z. R. HALLOCK

*QinetiQ North America, Slidell, Louisiana*

(Manuscript received 13 August 2010, in final form 11 January 2011)

### ABSTRACT

Closely spaced observations of nonlinear internal waves (NLIWs) were made on the outer continental shelf off New Jersey in June 2009. Nearly full water column measurements of current velocity were made with four acoustic Doppler current profilers (ADCPs) that were moored about 5 km apart on the bottom along a line approximately normal to the bathymetry between water depths of 67 and 92 m. Density profiles were obtained from two vertical strings of temperature and conductivity sensors that were deployed near each of the interior ADCP moorings. In addition, a towed ScanFish provided profiles and fixed-level records of temperature and salinity through several NLIW packets near the moorings. Several case studies were selected to describe the propagation of the NLIWs. One to three solitary waves of depression were observed in five selected packets. There were also occurrences of multiple-phase dispersive wave packets. The average propagation speed corrected for advection of the observed waves was  $0.51 \pm 0.09 \text{ m s}^{-1}$ . The waves were directed primarily shoreward ( $\sim$ northwestward) along the mooring line with average wavelengths and periods of about 300 m and 10 min, respectively. Wave amplitudes and energies decreased with decreasing water depth. The observed wave parameters can be locally described by a two-layer Korteweg–de Vries (KdV) model, except for the decreasing amplitudes, which may be due to shear-induced dissipation and/or bottom drag. The various complementary observations utilized in this study present a unique description of NLIWs.

### 1. Introduction

Nonlinear internal wave (NLIW) packets are commonly observed on continental shelves throughout the world. They are commonly thought to evolve from internal tides generated by the interaction of the barotropic tide with shelf-edge topography (Tang et al. 2007; Colosi et al. 2001) and to propagate shoreward when the interaction is with the shelfbreak. Characteristics of the waves, which are often described as packets of solitons, change as the water depth decreases. Their amplitudes can be quite large, and the waves can significantly impact acoustic, optical, and biogeochemical properties of the water column. A variety of techniques have been used to observe NLIWs such as using moored temperature and conductivity sensors, current meters (Colosi

et al. 2001; Duda et al. 2004; Hallock and Field 2005; MacKinnon and Gregg 2003), and high-frequency pressure sensors (Moum and Nash 2008). Shipboard measurements utilizing acoustic Doppler current profilers (ADCPs), conductivity–temperature–depth (CTD) profilers, and echo sounders have been used to make multiple transects across wave packets (e.g., Shroyer et al. 2008). NLIWs have been particularly well documented through satellite synthetic aperture radar (SAR) imagery (Jackson and Apel 2004). NLIWs can have a surface signature detectable by both ship and satellite radars in low wind conditions.

NLIWs were intensely studied as part of the Shallow Water Acoustics Experiment in the summer of 2006 (SW06) (Tang et al. 2007). This large multidisciplinary, multi-institution project off the coast of New Jersey focused on a hierarchy of processes, including internal tides, jets, density fronts, and NLIWs, that could affect U.S. Navy acoustic systems. SW06 objectives are focused on the structure, intensity, and direction of the internal wave

---

*Corresponding author address:* W. J. Teague, Naval Research Laboratory, Stennis Space Center, MI 39529.  
E-mail: teague@nrlssc.navy.mil

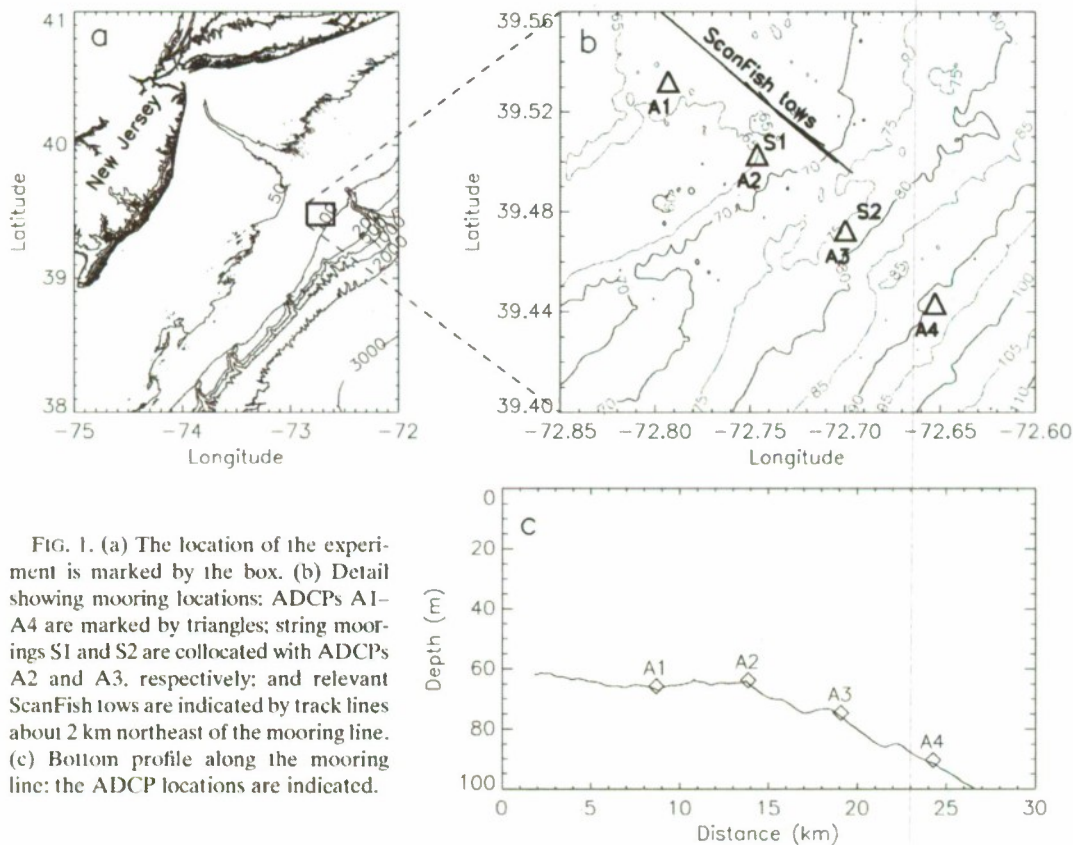


FIG. 1. (a) The location of the experiment is marked by the box. (b) Detail showing mooring locations: ADCPs A1–A4 are marked by triangles; string moorings S1 and S2 are collocated with ADCPs A2 and A3, respectively; and relevant ScanFish tows are indicated by track lines about 2 km northeast of the mooring line. (c) Bottom profile along the mooring line: the ADCP locations are indicated.

energy flux at the shelf break. During SW06, 62 moorings were deployed in a “T” geometry, and 5 of these moorings contained ADCPs, which provided nearly full water column velocity profiles. Three of these ADCP moorings were placed about 20 km apart along the likely propagation direction of the NLIWs while three were 10–15 km apart along a line perpendicular to the propagation direction. In addition, multiple ships were used to chase the packets, and gliders provided background observations. Shipboard observations included ADCP, X-band radar, temperature, salinity, and turbulence measurements.

Analyses of satellite imagery suggest that the width of a typical NLIW packet can range from several to more than 5 km (Porter and Thompson 1999). Thus far, this resolution has only been approached using a ship in chase mode collecting ADCP and CTD data. Moored instruments spaced at about 5 km or less would allow coherent measurements of waveforms and direct determination of phase and group velocities. Individual wave packets could be analyzed in detail for modal content and propagation characteristics. As part of the Naval Research Laboratory’s (NRL’s) field exercise near the shelf break off New Jersey, four ADCP moorings were spaced about 5 km apart along a line approximately

normal to the bathymetry (Fig. 1). The field measurements were performed as part of NRL Magnetic Ocean Forecasts project, whose main objective was to generate estimates of the ocean contribution to the magnetic noise from sources such as NLIWs. This topic is not addressed here. However, the field measurements provide the opportunity to analyze closely spaced mooring data and to fill in gaps of our understanding of NLIW dynamics not possible from earlier field studies. This paper focuses on analyses of several packets of large NLIWs that propagated through our mooring array.

In section 2, we describe the experiment and the observations made. In section 3, analyses of selected events in the data records and determination of wave characteristics are presented. Section 4 results are interpreted using first-order Korteweg–de Vries (KdV) theory for a two-layer system. Some conclusions are presented in section 5.

## 2. Observations

An extensive set of oceanographic measurements was made by the Naval Research Laboratory between 18 June and 1 July 2009 (corresponding to yeardays 168 and 181) during an R/V *Oceanus* cruise. The study area was

centered at about  $39.5^{\circ}\text{N}$  and  $72.7^{\circ}\text{W}$ , about 75 miles east of New Jersey (Fig. 1a). The instrumentation consisted of four ADCP moorings; two string moorings with temperature and conductivity; and a towed undulating body, *ScanFish*. Eight magnetometers were also deployed on the bottom next to the ADCP moorings but are not discussed in this paper. After all of the moorings were deployed, ship observations were made along a line parallel to the mooring line, offset about 2 km toward the northeast (Fig. 1b). The mooring line was avoided in order to not disturb the magnetic measurements.

#### a. ADCP moorings

Four ADCP moorings were deployed on the outer continental shelf off New Jersey and southwest of the Hudson Canyon at water depths ranging between 64 and 92 m (Fig. 1). The bottom profile along the mooring line is shown in Fig. 1c. Mooring A1 is located at a fairly flat portion of the bottom, A2 is located at the edge of the flat portion where the bottom profile begins to rapidly deepen, and A3 and A4 are located on the sloping portion of the profile. The moorings were deployed for about 9 days from 19 June 2009 (yearday 169) along a line oriented at  $310^{\circ}$  relative to true north and were approximately 5 km apart. The mooring line is approximately normal to the bathymetry. Numerous SAR images collected in this region during August and September 2006 in conjunction with SW06 suggest that NLIW crests are likely parallel to the isobaths along our mooring line.

The ADCPs were 307.2-kHz broadband “Workhorse Sentinels” manufactured by RD Instruments. They were deployed in trawl resistant mounts called “Barnys” after their barnacle-like shape (Perkins et al. 2000) that were lowered rather than free dropped to the bottom. They were then positioned so that the tilt of the transducer head from the vertical (ideal) orientation was minimized. The moorings were placed at depths ranging from about 67 to 92 m, with the seaward end of the mooring line near the shelf break of about 100 m. The ADCP heads were situated about 0.5 m off the bottom and recorded current profiles from about 4 m off the bottom to within about 4 m of the surface. Velocity measurements were recorded at a vertical resolution of 1 m every minute using a sampling scheme that used 70 pings distributed over the sampling period. The accuracy is  $0.5\% \pm 0.5 \text{ cm s}^{-1}$  and the random error, which is dependent on the depth-bin size, is reported as a standard deviation of  $1.6 \text{ cm s}^{-1}$ . Velocities were corrected for local magnetic variation. Each mooring also contained sensors for measuring temperature and pressure. The ADCP velocities are rotated ( $39.5^{\circ}$  clockwise) for the analyses here so that the east–west ( $U$ ) velocities are

oriented along the mooring line, where negative  $U$  is onshore and positive  $U$  is offshore.

#### b. String moorings

Two temperature–conductivity sensor strings (S1 and S2) were anchored on the bottom beneath a surface buoy approximately 300 m from the two interior ADCP moorings (A2 and A3; Fig. 1). Each string contained 10 Sea-Bird Electronics (SBE) 37 serial interface MicroCATs, high-accuracy conductivity, and temperature sensors. About half of the MicroCATs on each string contained pressure sensors. They were distributed in a telescoping scheme, starting with a spacing of 3 m at about 8 m below the surface and ranging to a spacing of 10 m at about 10 m above the bottom. Temperature is accurate to about  $0.002^{\circ}\text{C}$ , and conductivity is accurate to about  $0.003 \text{ mS cm}^{-1}$ .

#### c. ScanFish

Repeated tows of a *ScanFish* MK II manufactured by EIVA (<http://www.eiva.dk>) were made along a line parallel to the mooring line (Fig. 1) throughout the cruise period, shifted by 2 km northeast of the mooring line to minimize interference with the deployed magnetometers. The *ScanFish* is a towed undulating vehicle that can fly in undulating, fixed depth, and terrain following modes. It records numerous physical and optical parameters, but just the temperature, conductivity, and pressure data are used in analyses here. The *ScanFish* was typically towed at 5.5 kt throughout the cruise. Both level and undulating modes were used to sample NLIW packets.

#### d. Hydrography

CTD stations were taken at mooring sites A1–A3 on 20 June (yearday 170) and near mooring sites A1–A4 along the *ScanFish* line, approximately 2 km northeast of the moorings, on 25 June (yearday 175). Each CTD station consisted of three consecutive downcasts, made to just above the bottom. On 20 June, the mixed layer was shallow, 5–10 m in depth, and the seasonal thermocline ranged from about 10 to 25 m in depth. Well-mixed bottom layers that were about 5 m thick were observed at A1 and A2. At A3, a well-mixed layer about 15 m thick was located just above a near-bottom density gradient where density  $\sigma_t$  changed by  $0.3 \text{ kg m}^{-3}$  over the bottom 5 m. Brunt–Väisälä frequencies ranged from 26 to 31 eph in the seasonal thermocline and from 16 to 19 eph near the bottom. By 25 June, the mixed layer had eroded and the seasonal thermocline weakened and deepened. Well-mixed bottom layers disappeared at A4, A3, and A2. However, the bottom layer at A1 thickened to about 15 m and was less dense by about  $0.2 \text{ kg m}^{-3}$



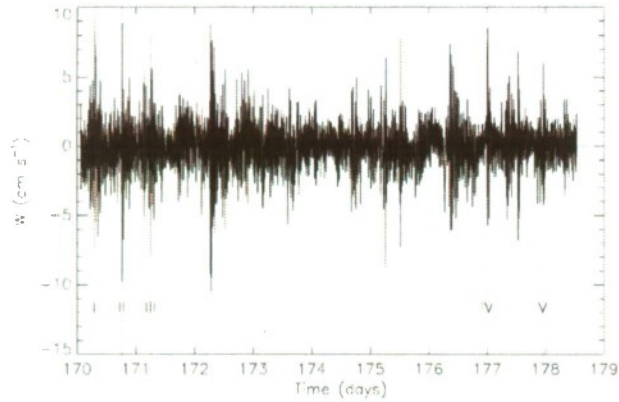


FIG. 3. Vertical velocity  $W$  at 23 m at ADCP 2. Vertical dotted lines indicate the 5 cases for the ADCP soliton events.

been recovered by the time cases V and VI were observed. Packets were not evident at A4 during cases I and IV.

Vertical velocity from ADCP 2 at the depth of maximum variance is plotted in Fig. 3, where a number of large-amplitude events are evident in the record. A few of these were selected for analysis based on three criteria: relatively large amplitude; resemblance to simple internal solitary waves; and appearance in at least three of the ADCP records, thus allowing tracking and propagation speed determinations. The mooring line was chosen to be parallel to expected NLIW propagation direction. Clearly, this direction can vary for different waves or packets of waves passing a given point. If we take the  $x$  along the mooring line and  $\theta$  as the departure of wave direction from the  $x$  axis, then (for plane wave fronts) the apparent phase speed (along  $x$ )  $C' = C/\cos\theta$ , where  $C$  is the actual phase speed. This means that the observed speeds will be greater than or equal to the actual speed. For  $\theta$  up to about  $25^\circ$ , the ratio  $C/C'$  is greater than 0.9, so small directional uncertainties will not result in large errors in estimates of  $C$ . Five cases (I–V; see Table 1), each consisting of 1–3 closely spaced solitary wave events, are indicated in Fig. 3. A total of 10 solitons were tracked through most of the moorings, resulting in 36 observations at the four ADCP locations and 4 observations at S1 and S2. Case I and IV solitons were not seen at A4. The case IV solitons (2) were also observed twice with the ScanFish. The prominent event near yearday 172.5 is predominantly a packet of large-amplitude internal waves rather than well-defined solitary waves. Case VI consisted of two ScanFish tows, near the A2 location, conducted after recovery of all moorings. We analyze the observations in the light of a two-layer, first-order KdV model (Small 2001; Holloway 1987; Gear and Grimshaw 1983).

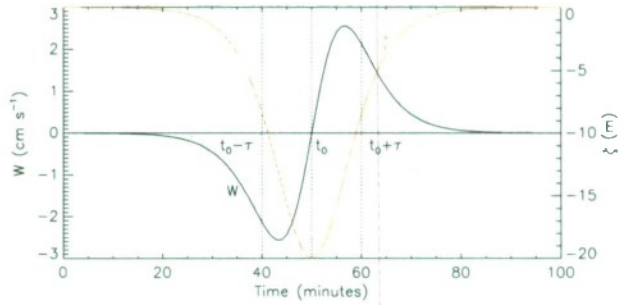


FIG. 4. Schematic of KdV soliton of depression (red) and associated vertical velocity (black).

#### a. Phase speeds

A number of factors determine apparent propagation speeds, along a particular direction, of NLIWs (Small 2001; Gear and Grimshaw 1983; Phillips 1969). These include stratification, water depth, wave amplitude, actual propagation direction, and advection (Doppler shift) and shear by the ambient flow in which the waves are embedded.

Phase speeds of a number of selected NLIWs observed in the ADCP velocities are estimated using the times that a particular event passes each ADCP and the distance between the moorings. Because the internal waves are superimposed on the ambient, depth-averaged low-frequency flow, mostly the barotropic tide, a Doppler correction is made so that calculated speeds are relative to this ambient flow. The events analyzed were selected by examining records of vertical velocity  $W$  that were robust and appeared in at least two data records. The characteristic shape of a first-order KdV soliton of depression (Holloway 1987; Gear and Grimshaw 1983) is described by

$$\zeta(x, t) = a \operatorname{sech}^2\left(\frac{x - Ct}{L}\right) \quad \text{and}$$

$$W = \frac{d\zeta}{dt} = \frac{2aC}{L} \operatorname{sech}^2\left(\frac{x - Ct}{L}\right) \tanh\left(\frac{x - Ct}{L}\right), \quad (1)$$

where  $\zeta$  is elevation (interface displacement for a two-layer system),  $a < 0$  for a soliton of depression,  $L$  is a length scale, and  $C$  is propagation speed. For first-vertical-mode waves, the horizontal velocity is proportional to  $\zeta$  and changes sign near the depth of maximum  $W$ . Hence,  $U$  can also be described by the  $\operatorname{sech}^2$  function. For Eulerian measurements, we can set  $x = 0$  and define a time scale  $\tau = L/C$  and reference time  $t_0$  to simplify the following. These functions are plotted in Fig. 4 with  $t_0 = 50$  min and  $\tau = 10$  min. The period of the soliton can be defined as  $3.6\tau$ , the point at which the magnitude of  $\zeta$  falls to 10% of the maximum (Holloway 1987); likewise,

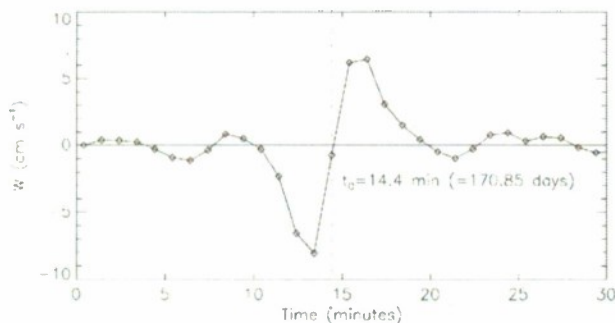


FIG. 5. Vertical velocity from ADCP A1 (case II). The abscissa is in minutes for easy comparison with the analytical plot in Fig. 4. Diamonds on the curve denote actual data samples (1-min interval).

a wavelength is defined as  $\lambda = 3.6L$ . It should be noted that the amplitude of  $W$  is proportional to  $a/\tau$ . When a soliton of depression arrives at a moored measuring system,  $W$  first goes negative to a minimum value, then crosses zero to a maximum, and subsequently decays back to zero. We define the time of arrival of a soliton event at a mooring as  $t_0$ , where  $W$  crosses zero from the minimum to the maximum. An example of such an event in a moored current record is shown in Fig. 5. Time in relative minutes is shown to more easily compare with Fig. 4. The actual value of  $t_0$  is yearday 170.85.

The event in Fig. 5 was detected earlier in the other three ADCP records, from locations southeastward from A1. There were also two additional events following the one shown that appeared in all four records. The northwestward progression of these events is shown in Fig. 6; a somewhat longer time interval for all four records are plotted to include the three events (labeled a–c). The times of the events and distances between the moorings ( $\sim 5$  km) yield apparent propagation speeds between respective mooring locations. The three events moving from A4 to A3, from A3 to A2, and from A2 to A1 yield nine estimates of propagation speed. These range from  $-0.74$  to  $-0.44$   $\text{m s}^{-1}$ . The calculated speeds are interpreted as soliton phase speed  $C$  superimposed on the ambient flow (due primarily to the barotropic tide). The ambient flow is estimated by low-pass-filtered, depth-averaged currents (LF currents) from the ADCP records. The half-amplitude point of the filter is set at a period of 2 h. For illustration, a further average of rotated LF current, over the four ADCP records, is plotted in Fig. 7. Fluctuations are due mainly to the M2 tide, but there is also a southeastward mean as well. Actual corrections for speed calculations were made as follows, for example: An event passes from A3 to A2 in a time interval  $\Delta t$  over the distance  $\Delta x$  ( $\sim 5$  km). We calculate an average LF current  $\overline{\overline{U}}_{32}$ , where the double overbar indicates averaging the LF flow over A2 and A3 and over

$\Delta t$ . Then, we have  $\Delta x = (C + \overline{\overline{U}}_{32})\Delta t$ . Solving for  $C$  yields a corrected phase speed. For the events in Fig. 6,  $C$  ranges from  $-0.65$  to  $-0.48$   $\text{m s}^{-1}$ . Here,  $C$  is an estimate of the intrinsic internal wave phase speed. We note that this correction does not address phase mean vertical shear, which can also affect the phase speeds and other wave properties (Alford et al. 2010).

In all, five cases (of which the above is case II) captured by the ADCP moorings, some with subcases (a, b, etc.), were selected for a total of 10 solitons passing at least three of the moorings. Each of the 36 events observed resemble Fig. 5 and are hence solitons of depression. Means and standard deviations (for each location) of both advection-corrected and uncorrected  $C$  estimates are plotted in Fig. 8. The uncorrected speeds show an increase in (negative) amplitude with increasing depth; the variability suggests that this may not be a significant change. The corrected speeds, however, show less change and do not follow the depth profile. We conclude that the changes are not significant and that the composite mean of  $-0.51 \pm 0.09$   $\text{m s}^{-1}$  is a best estimate of the phase speed along the mooring line, based on the selected events from the ADCP observations. Furthermore, this mean value is not significantly different from the mean for the uncorrected speeds ( $-0.54 \pm 0.11$   $\text{m s}^{-1}$ ). Horizontal current velocities associated with the wave events were nearly all well below our average phase speed of  $0.51$   $\text{m s}^{-1}$ . Exceptions included several isolated points for case IV, which may be the result of noisy data and near the surface for case V; the latter may indicate periods of convective instability.

Two ScanFish tows were made in the constant depth mode at about 30 m just east of mooring A2 (Fig. 1b), concurrent with the events of case IV. A NLIW packet was first crossed during a shoreward-directed tow that was immediately followed by a seaward-directed tow. Shown in Fig. 9 is  $\sigma_t$  from tows 25 and 26 as a function of along-track distance. The features marked a and b correspond to case IV events in the ADCP records. The location of mooring A2 is indicated by the vertical dotted line. The peaks at a and b are well defined by density, and their shapes were very consistent between the tows. Note that the a and b negative peaks are about 500 m apart and are slightly closer together for the seaward tow, which is consistent with wave movement to the left. Internal wave activity is apparent after the NLIW packets pass but does not appear correlated between the tows. Density data from the string mooring (S1; not shown) show that density contrast would have been greater if the level tow had been made between 10- and 20-m depths. Distances and corresponding times for the selected features in Fig. 9 are listed in Table 2. The advective correction here is  $-0.15$   $\text{m s}^{-1}$ . The data in Table 2

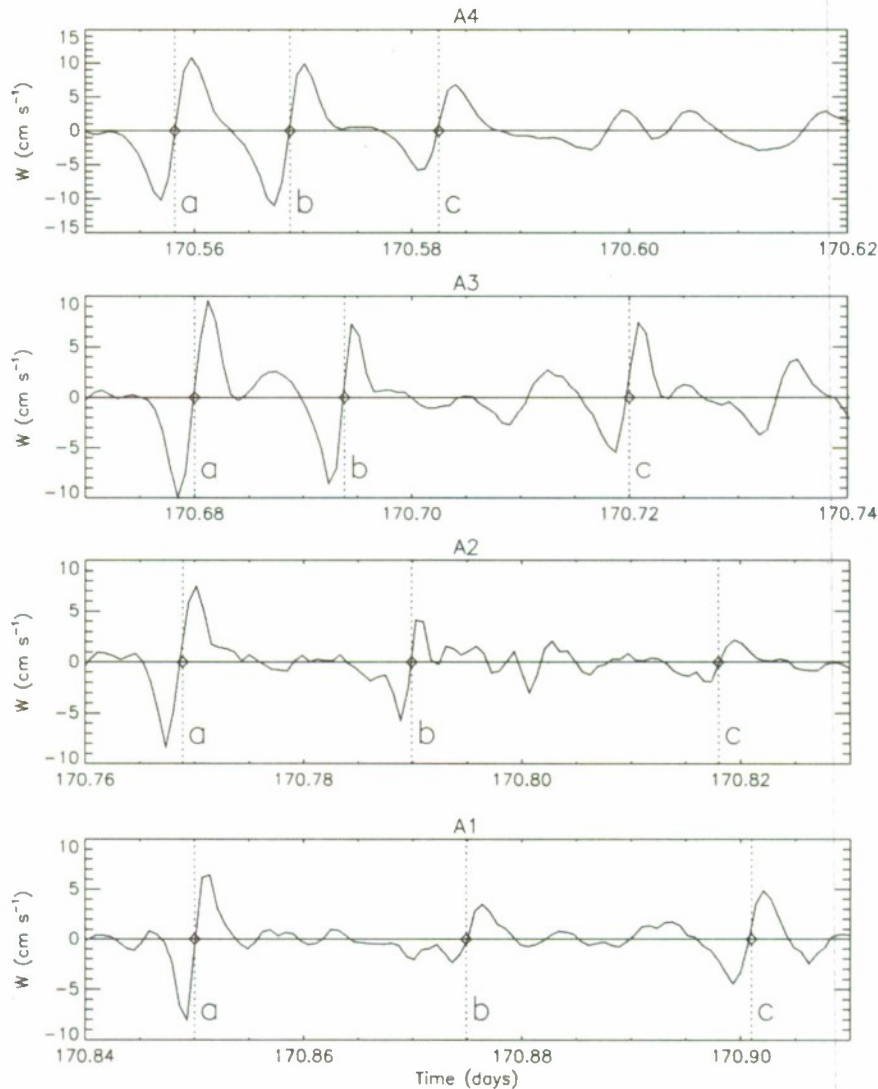


FIG. 6. Vertical velocity  $W$  at ADCP locations (case II), at the depth of the maximum  $W$  time variability, for time intervals showing three soliton events (labeled a–c) propagating from A4 (offshore) to A1 (onshore).

yield propagation velocities of  $-0.41$  and  $-0.43$   $\text{m s}^{-1}$  for a and b, respectively. Correcting for the LF advection,  $C$  becomes  $-0.26$  and  $-0.28$   $\text{m s}^{-1}$ . These values are consistent with ADCP-based speeds for case IV but are lower than the averages in Fig. 8.

After all moorings were recovered, two ScanFish tows were made near the A2 location. Figure 10 shows  $\sigma_r$  from tows 42 and 43 as a function of along-track distance; we denote this as case VI, which is possibly the result of a solitary wave breaking into a train of dispersive waves. The peak-connecting lines are a best guess at corresponding features in the wave packet, from tow 42 to 43. As in Fig. 9, the features are more compressed for the seaward tow, consistent with shoreward wave movement. Furthermore, the wave packet has

significantly evolved between tows 42 and 43; on the other hand, it may have interacted with another wave. Distances and times (from similar plots versus time) for the 14 features yield 14 estimates of  $C$ . Note that the time intervals between feature positions in tows 42 and 43 increase shoreward (with decreasing distance) because of the respective tow directions. The  $C$  estimates show an increase with increasing distance, but this may be biased by the aforementioned changing interval. The mean of the 14 estimates, corrected for advection, is  $C = -0.54 \pm 0.07$   $\text{m s}^{-1}$ , close to the ADCP-derived average speed of  $0.51$   $\text{m s}^{-1}$ . MacKinnon and Gregg (2003) find wave speeds about the same as we find (about  $-0.5$   $\text{m s}^{-1}$ ) from observations made in 1996 near our experimental area. However, Shroyer et al. (2008), based

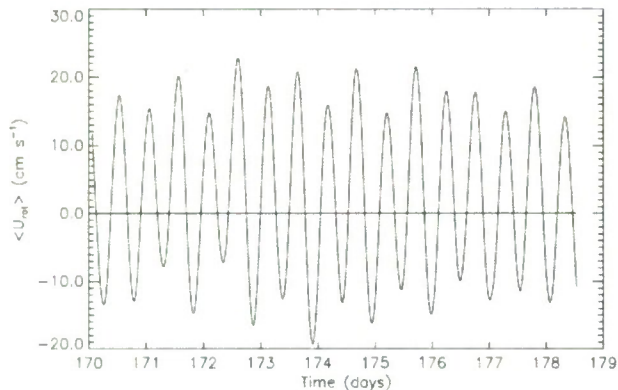


FIG. 7. Overall depth- and horizontally averaged low-frequency, rotated current.

on measurements made in 2006 in the same general area, report phase speeds for NLIWs closer to  $0.7 \text{ m s}^{-1}$ .

*b. Wave properties*

We now examine case III in some detail, where a pair of solitary waves is seen moving past the four ADCP moorings. Horizontal velocity  $U$  (rotated so that positive  $U$  is seaward along the mooring line) and vertical velocity  $W$  for ADCPs A1–A4 are shown in Fig. 11; note that the maximum depths shown in these plots are less than the actual water depths of 67, 65, 76, and 91 m for A1–A4, respectively. The time intervals of the plot panels are 0.07 day (about 100 min) for the respective periods containing two propagating solitons. The observed propagation speed of event a is slightly greater than that of event b. Note that  $U$  changes sign near 20-m depth, near the maximum in the magnitude of  $W$ . The negative (positive)  $U$  above (below) the zero level is consistent with propagation in the negative  $x$  direction or shoreward along the mooring line for a first-mode wave. Amplitudes of the waves decrease at A2 and A1 relative to A3 and A4, and smaller wavelike features appear between a and b, suggesting possible breaking or fissioning of the solitons (Djordjevic and Redekopp 1978). Temperature, salinity, and density for case III at A2 and A3 are shown in Fig. 12 (as stated above, maximum depths shown are less than actual water depth), where vertical displacements of 10–20 m are evident, particularly for temperature and density. The event times from the ADCP records are indicated in Fig. 12 by vertical dashed lines. The time lags at the string moorings reflect the slightly different positions ( $\sim 200 \text{ m}$ ) of the moorings. The appearance of two additional small waves at S1 (A2) is consistent with what is seen in Fig. 11.

At the depths of maximum variance in  $W$ , short (20 min) segments of data centered on the points where  $W$  crosses 0 (negative to positive; e.g., at  $t_0$  in Fig. 6) were

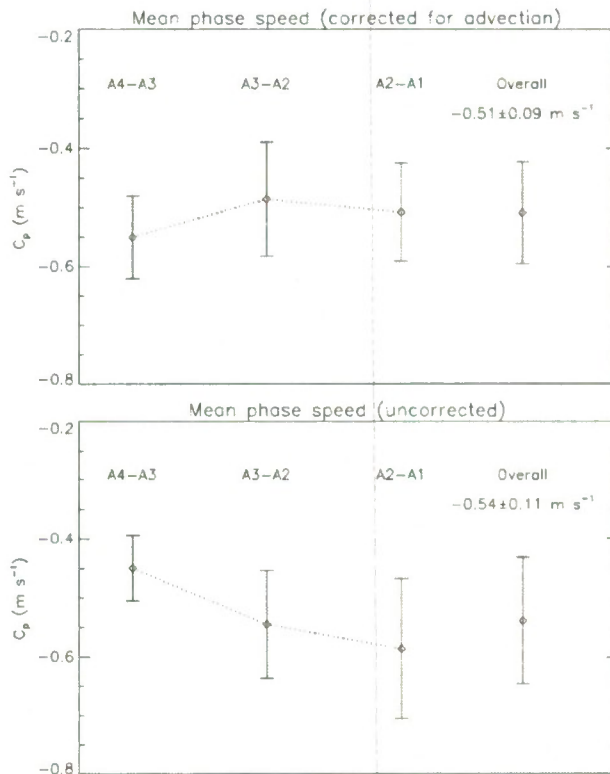


FIG. 8. Mean phase speeds based on arrival times of selected internal soliton events in the records of vertical velocity at the ADCP locations: (top) corrected for advection and (bottom) uncorrected.

fitted by least squares to the functional form for  $W$  in Eq. (1) to determine the parameters  $a$  and  $\tau$  ( $=L/C$ ).

Recall [from Eq. (1)] that, for Eulerian data,

$$W = -\frac{2a}{\tau} \text{scch}^2\left(\frac{t-t_0}{\tau}\right) \tanh\left(\frac{t-t_0}{\tau}\right). \quad (2)$$

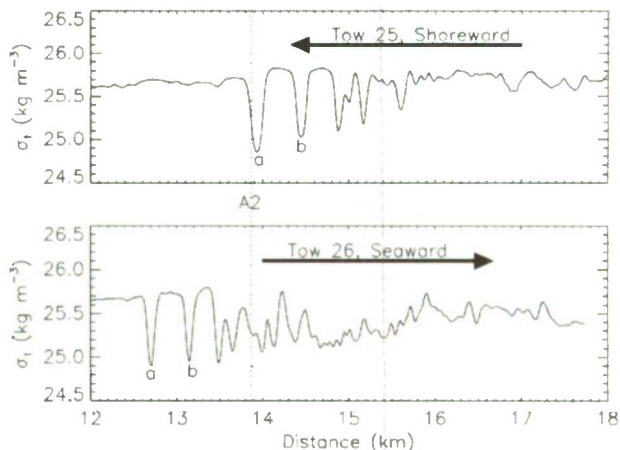


FIG. 9. ScanFish level tows (top) 25 and (bottom) 26. The location of ADCP A2 is indicated by a vertical dotted line.

TABLE 2. Times and distances for case IV events in ScanFish tows 25 and 26.

	Tow 25 (a)	Tow 26 (a)	Tow 25 (b)	Tow 26 (b)
Time (days)	176.9945	177.0294	176.9966	177.0312
Distance (km)	13.93	12.70	14.44	13.15

If  $a_w$  is the peak amplitude of the fitted  $W$ , then

$$a = -\frac{a_w \tau}{2} / \max \left[ \operatorname{sech}^2 \left( \frac{t - t_0}{\tau} \right) \tanh \left( \frac{t - t_0}{\tau} \right) \right] \cong -\frac{a_w \tau}{2 \times 0.3849}. \quad (3)$$

However, the time scale resulting from the fitting algorithm is biased by the advection (as in the determinations of  $C$ ) and hence needs to be corrected before (3) can be used. That is, if the LF current is in the direction of propagation, the observed time scale  $\tau'$  will be shorter than the intrinsic  $\tau$  and vice versa. We can then write

$$C\tau = L = (C + U)\tau' \quad \text{or} \quad \tau = \left( 1 + \frac{U}{C} \right) \tau'. \quad (4)$$

In Fig. 13, we show the 20-min segments of  $W$  for the two events of case III at the four ADCP locations. On each subpanel is listed  $a_w$ , the correlation of the fit of (2) to the data and  $\tau'$ . The amplitudes clearly decrease going from A4 to A1. The least squares fitting procedure was performed on data for the five cases yielding a total of 36 determinations of  $a_w$  and  $\tau'$ . Correlations for all 36 events are  $>0.81$  and most are  $>0.90$ . Advection corrections (4) were made by using the average value of  $C = 0.51 \text{ m s}^{-1}$  and the displacement amplitude  $a$  calculated using (3). Calculated  $\tau$  and  $a$  are relatively insensitive to the variability of  $C$  about the average used. On the other hand,  $L$  depends directly on  $C$ , so the variability of  $L$  depends on that of both  $C$  and  $\tau$ . Overall average soliton period ( $T = 3.6\tau$ ) is  $\sim 10$  min, and wavelength (for this  $C$ ;  $\lambda = 3.6L$ ) is  $\sim 300$  m (as in Holloway 1987). Means and standard deviations of  $a$  and  $a_w$  at each location are shown in Fig. 14, and the means are listed in Table 3; as indicated in Table 1, there are 10 samples each for A1–A3 but only 6 for A4. Although the variability at each location is high, a decrease in amplitude of both vertical displacement and velocity with decreasing water depth is suggested. This change with depth cannot be directly explained with the simple model presented here; below, we examine bottom friction and the potential for shear instability in the pycnocline to explain the amplitude decrease. Furthermore,

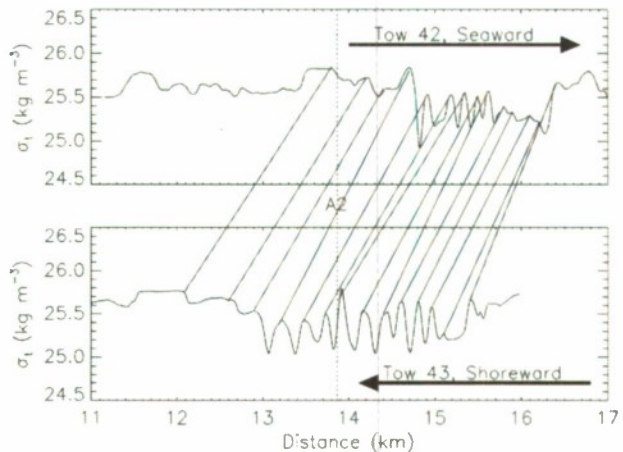


FIG. 10. ScanFish level tows (top) 42 and (bottom) 43. The location of ADCP A2 is indicated by a vertical dotted line. Corresponding NLIW peaks are connected by solid lines.

these displacement amplitude magnitudes  $|a|$  are at or above a maximum  $a_{\max}$  (means also listed in Table 3) for KdV (and extended or second-order KdV) waves (Helfrich and Melville 2006; Small 2001).

Horizontal velocity  $U$  suggests a two-layer structure (Fig. 11), where  $\zeta$  is the height of the interface between the layers, of thickness  $h_1$  and  $h_2$ . Here,  $\zeta$  can be estimated by integrating vertical velocity: that is,  $\zeta = \int W(-h_1, t) dt$ . For case III,  $\zeta$  excursions at A2 and A3 are comparable to the pycnocline depressions in the bottom panels of Fig. 12. To simplify comparison to KdV theory, we compute layer-averaged velocities  $U_1$  (upper layer) and  $U_2$  (lower layer). Because the zero-crossing depth varies among the events, the depth interval between 15 and 30 m is excluded in the calculation. Correlations between  $U_2$  and  $\zeta$  for all 36 selected events are strongly negative, consistent with shoreward propagation. The resulting series are fit to  $\operatorname{sech}^2[(t - t_0)/\tau]$  to determine amplitude for each event period. Average amplitudes for  $U_1$  and  $U_2$  at each location are plotted in Fig. 14e. The  $U_1$  layer averages are quite noisy in the latter part of the record, and correlation values for the least squares fit are correspondingly low. Hence, only correlations above 0.8 are used in the averages shown in Fig. 14e. This value represents the lowest correlation found for the  $W$  fits, and the  $U_2$  correlations all exceed this value. This problem is most noticeable for A4, where only four events have acceptable correlations. The numbers of events included in the averages are indicated in the figure. The signs of the averages shown are consistent with shoreward movement.

### c. Energetics

It is useful to calculate energies associated with the observed NLIW events. We assume that the wave available

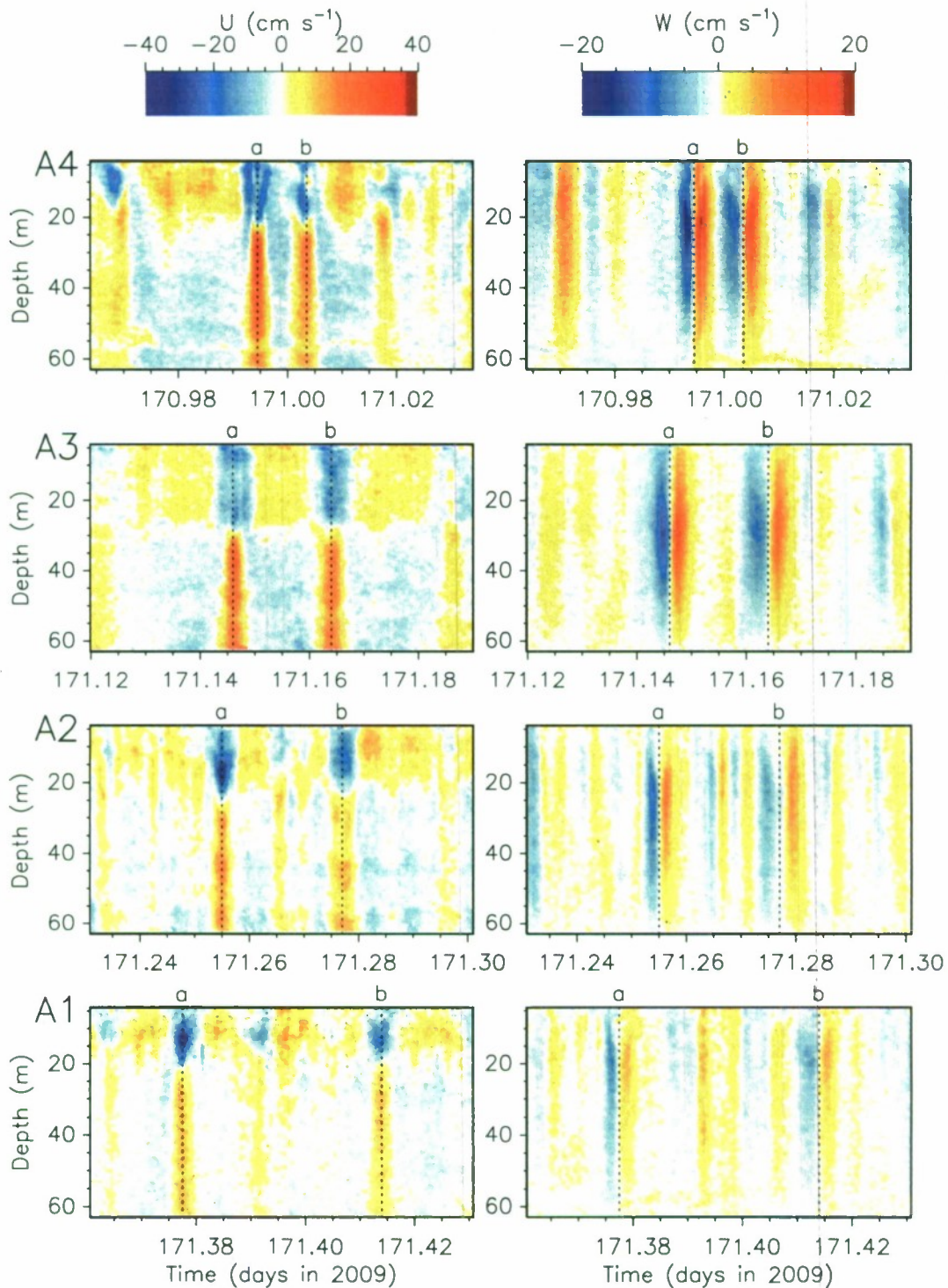


FIG. 11. Rotated, (left) high-pass-filtered horizontal velocity  $U$  and (right) vertical velocity  $W$  for case III from (top to bottom) the four ADCP records. The features marked a and b can be tracked through all four moorings.

potential energy (APE) and kinetic energy (KE) are approximately equal; hence, the total energy per unit distance along the crest (perpendicular to propagation direction) of internal waves can be taken as  $\sim 2 \times \text{APE}$ .

It is likely, however, that the kinetic energy is greater than the available potential energy for large-amplitude solitons. The ratio  $\text{KE}/\text{APE}$  may be closer to 1.5 (Moum et al. 2007; Klymak and Moum 2003; Klymak et al. 2006),

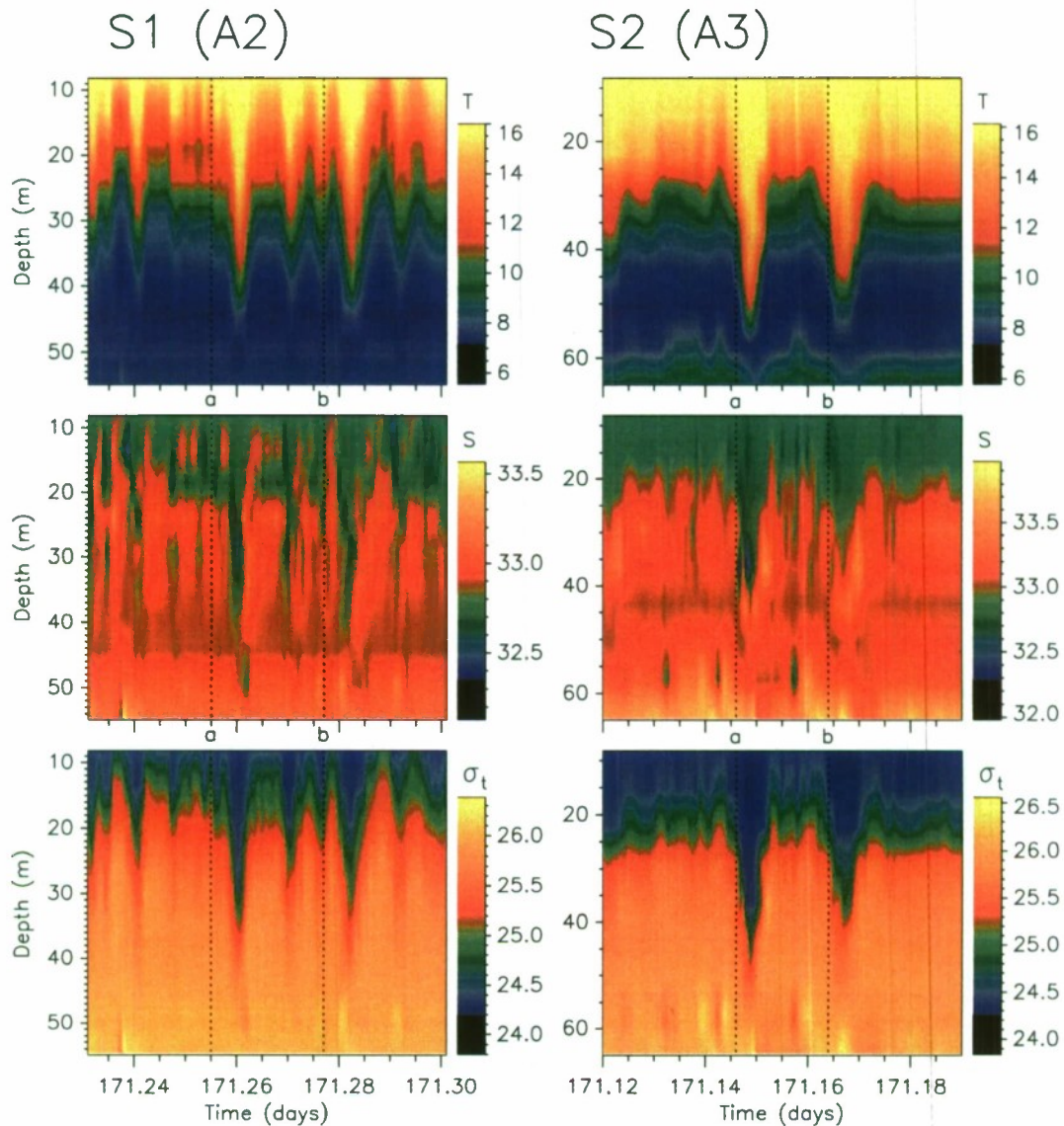


FIG. 12. (top to bottom) Temperature, salinity, and  $\sigma_t$  from conductivity-temperature string moorings (left) S1 and (right) S2 for case III. The time intervals displayed are as in Fig. 11. Vertical dashed lines mark corresponding event times in ADCP records (see Fig. 11).

so the equipartition assumption may underestimate the total energy. That said, the total energy can be expressed (in a two-layer system) as  $E_\zeta \cong 2\text{APE} = \int_{x_1}^{x_2} \Delta\rho g \zeta^2(x) dx$  (Phillips 1969), where  $\Delta\rho = \rho_2 - \rho_1$  is the layer density difference (Table 3) and  $x$  represents distance relative to the moving waveform. The units of  $E_\zeta$  are  $\text{J m}^{-1}$ . The limits  $x_1$  and  $x_2$  are chosen to include the features of interest:  $x_1$  is selected to be 7 min (equivalent distance of 210 m for a phase speed of  $0.5 \text{ m s}^{-1}$ ) prior to the 0 crossing for  $W$  (see Fig. 5), and  $x_2$  is selected at 7 min prior to the 0 crossing for  $W$  in the following event, to include possible smaller waves resulting from breakup or fission of the first wave (see section 3b). This

approach limits the calculation of energy to cases having at least two events (e.g., IIIa-IIIb yields one result for each of the four ADCP locations). In all, there are five energies each for A1-A3 and three at A4. There is considerable scatter in the results, but averages for each location are shown in Table 3. Note that the mean energies for A1 and A2 are lower than those for A3 and A4, suggesting a transition between A2 and A3. Overall means and standard deviations for these location pairs are  $E_{12} = 0.13 \pm 0.09 \text{ MJ m}^{-1}$  and  $E_{34} = 0.31 \pm 0.11 \text{ MJ m}^{-1}$ ; the difference is significant. The NLIW energies estimated here are larger but of the same order as most of those reported by Shroyer et al. (2010) for observations

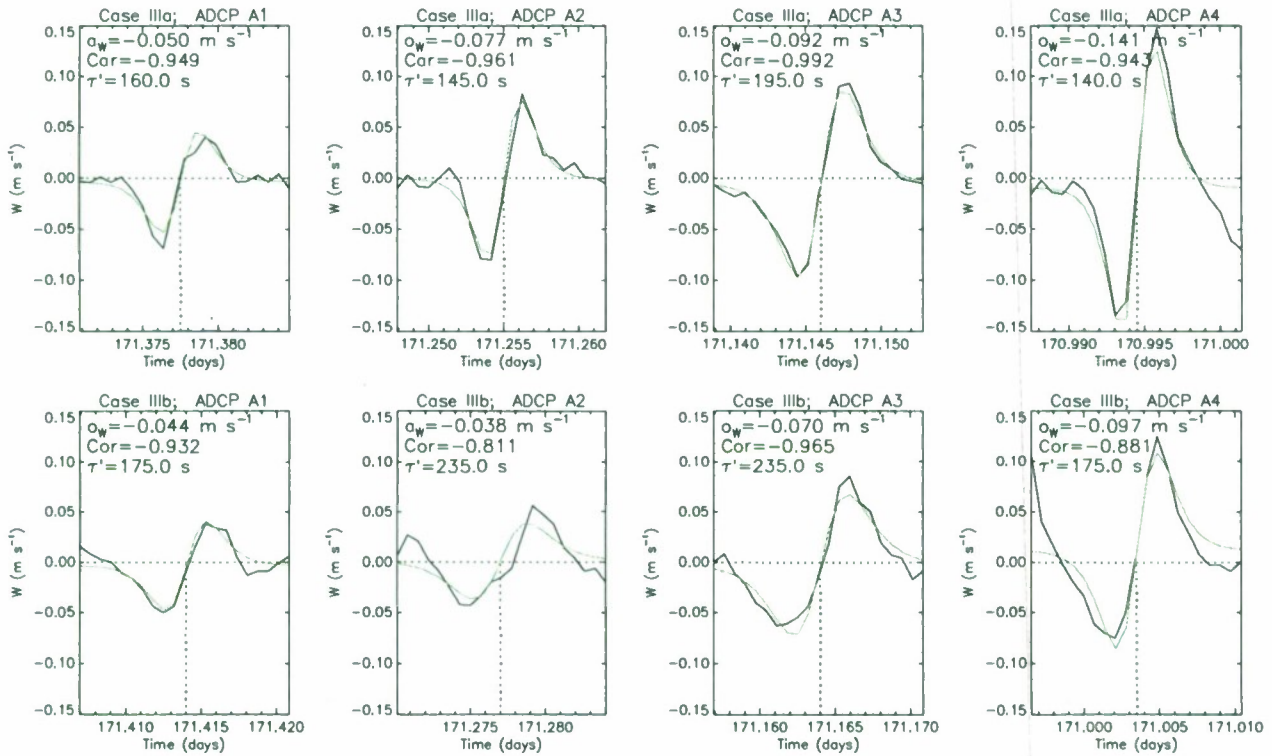


FIG. 13. The unfitted  $W$  (black) and fitted (green; see text) at depth of maximum variance for the two events [(top) a and (bottom) b] for case III and (from left to right) A1 to A4. Fitted amplitude  $a_w$ , correlation with observed data, and observed time scale  $\tau'$  are listed in each panel.

made in 2006 just to the south of our experimental area. The change in energy might be due to frictional effects. To estimate dissipation between these two areas, we first calculate energy flux averaged over the feature of interest,  $F = CE_{\bar{\epsilon}}/(x_2 - x_1)$  (Moum et al. 2007). We divide by  $x_2 - x_1$  to give a horizontal mean versus integrated energy;  $F$  then has units of  $\text{W m}^{-1}$ . The fluxes thus calculated for each event are then averaged as above to yield  $F_{12} = 63.4 \text{ W m}^{-1}$  and  $F_{34} = 274.2 \text{ W m}^{-1}$ . The dissipation rate is estimated as  $D = (F_{34} - F_{12})/\rho\Delta x\bar{h} = 2.75 \times 10^{-7} \text{ W kg}^{-1}$ , where  $\Delta x = 10 \text{ km}$  (distance between a point midway between A1 and A2 and a point midway between A3 and A4),  $\rho = 1025 \text{ kg m}^{-3}$ , and  $\bar{h} = 75 \text{ m}$  (the average depth for the moorings; see Fig. 1c for reference). This value of  $D$  is two orders of magnitude larger than that found by Hallock and Field (2005) from data in a nearby area, but their value was based on a long-term mean flux and averaged over a larger horizontal area; they stated that dissipation rates averaged over individual NLIW events would likely be much greater. MacKinnon and Gregg (2003) found different dissipation values (about  $3 \times 10^{-8} \text{ W kg}^{-1}$ ); they also used different spatial limits for averaging. Shroyer et al. (2010) report dissipative loss values of  $50\text{--}100 \text{ W m}^{-1}$  for NLIWs, comparable to our  $F_{34} - F_{12} = \sim 200 \text{ W m}^{-1}$

(they calculated dissipative loss as density times the dissipation rate integrated vertically over the depth of the pycnocline and horizontally over the wave). The dissipation may be the result of a combination of both shear instability in the pycnocline and bottom frictional drag on the horizontal velocity associated with the waves (Shroyer et al. 2010; Moum et al. 2007; Klymak and Moum 2003; Dewey and Crawford 1988).

Richardson number  $Ri$  calculations based on the density profiles from the string moorings (S1, S2) and velocity shear from ADCPs A2 and A3 show some tendency for instability ( $Ri < 0.25$ ) mainly shallower than 25 m but more at A2 than at A3. A quite crude estimate of dissipation can be made from  $Ri$ -based mixing formulations (e.g., Large et al. 1994; Zaron and Moum 2009). The  $K$ -profile parameterization (KPP) formulation of Large et al. (1994) expresses the eddy diffusivity,  $K_p = K_0[1 - (Ri/Ri_0)^2]^3$  for  $Ri \leq 0.7$  and  $K_p = 0$  for  $Ri > 0.7$ , where  $Ri_0 = 0.7$  and  $K_0 = 5 \times 10^{-3} \text{ m}^2 \text{ s}^{-1}$ . We noted that diffusivity is high at S1 compared to S2, suggesting that more mixing activities are likely at S1 than that at S2. An estimate of dissipation rate can be obtained, because  $K_p = 0.2\varepsilon/N^2$  (Osborn 1980). Dissipation rate is then  $\varepsilon \approx 5K_pN^2$ , which is on the order of  $10^{-6} \text{ W kg}^{-1}$ , but dissipation is smaller for deeper depths, where  $Ri > 1$  (for

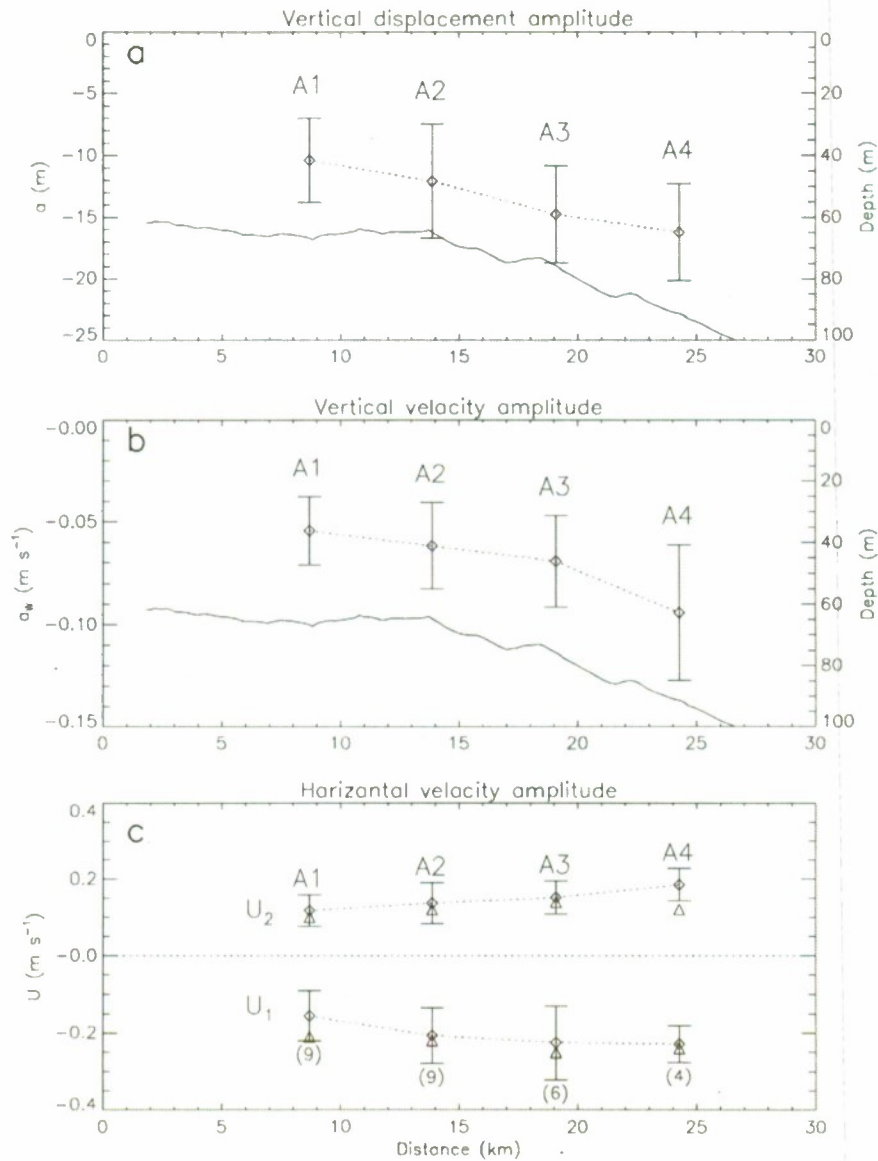


FIG. 14. Mean ( $\pm 1$  standard deviation) amplitudes at each ADCP location (diamonds connected by dotted lines). (a) Displacement amplitude  $a$ . (b) Fitted vertical velocity amplitude  $a_w$ . The bathymetric profile along the mooring line is also shown (with right ordinate axis). (c) Upper- and lower-layer horizontal velocity amplitudes  $a_{U1}$  and  $a_{U2}$ ; numbers in parentheses for  $U_1$  indicate how many events are included in the respective statistics (see text). Triangles denote derived amplitudes  $b_{U1}$  and  $b_{U2}$  from the two-layer model (Table 3).

most of the water column), and depth-averaged dissipation is more likely one order of magnitude smaller than at the shallower depth bins. A water column average dissipation is then (assuming about 5-m-thick pycnocline)  $D_{\text{shear}} = 5\epsilon/75 \approx 7 \times 10^{-8} \text{ W kg}^{-1}$ .

Bottom dissipation rates were computed by assuming that the “wall layer” or the constant stress layer exists between the sea bed and the nearest ADCP bin (see, e.g., Johnson et al. 1994; Wijesekera et al. 2010). This is a very rough estimate, because this boundary layer

thickness might be smaller than the assumed height (i.e., to the height of the first bin of ADCP, about 4 m). The friction velocity was estimated for a hydrodynamically smooth bottom (e.g., for mud flats) with a bottom roughness length scale of about  $z_0 = 0.01 \text{ mm}$  (e.g., Sutton 1953). These dissipation estimates can be treated as lower bounds, because  $z_0$  can be higher than 0.01 mm. Calculated total dissipations exhibit strong time variability, ranging from  $0.1 \times 10^{-6} \text{ W kg}^{-1}$  to  $1.2 \times 10^{-6} \text{ W kg}^{-1}$  at  $\sim 12$ -h (and shorter) periods, roughly corresponding

TABLE 3. Two-layer parameters. The top 10 rows are based on observations. Rows 11–17 are derived using the first-order KdV model [Eqs. (5)–(8)].

	A1	A2	A3	A4
$H$ (m)	67	65	76	91
$h_1$ (m)	22	23	27	30
$h_2$ (m)	45	42	40	61
$\Delta\rho$ ( $\text{kg m}^{-3}$ )	1.38	1.30	1.25	1.01
$a_w$ ( $\text{m s}^{-1}$ )	-0.05	-0.06	-0.07	-0.09
$a$ (m)	-10.4	-12.1	-14.8	-16.2
$a_{\text{max}}$ (m)	-11.4	-9.4	-10.8	-15.7
$u_{U1}$ ( $\text{m s}^{-1}$ )	-0.15	-0.21	-0.23	-0.23
$u_{U2}$ ( $\text{m s}^{-1}$ )	0.12	0.14	0.15	0.19
$E_\zeta$ ( $\text{MJ m}^{-1}$ )	0.16	0.10	0.29	0.33
$C_0$ ( $\text{m s}^{-1}$ )	-0.44	-0.43	-0.46	-0.44
$C$ ( $\text{m s}^{-1}$ )	-0.49	-0.48	-0.51	-0.50
$\lambda$ (m)	266	265	305	339
$T$ (min)	8.97	9.23	9.97	11.28
$b_{U1}$ ( $\text{m s}^{-1}$ )	-0.21	-0.22	-0.25	-0.24
$b_{U2}$ ( $\text{m s}^{-1}$ )	0.10	0.12	0.14	0.12
$E$ ( $\text{MJ m}^{-1}$ )	0.14	0.18	0.30	0.33

to semidiurnal and internal wave periods. A similar calculation based on LF series (tidal and longer periods) yields a dissipation of about 30% of the total. As for the thermocline dissipation, we find an average value on the order of  $10^{-6}$  W  $\text{kg}^{-1}$ . Again, this value is for the  $\sim 4$ -m assumed bottom boundary layer, so it would be about 10% of this value if averaged over the entire water column. This yields about the same value for  $D_{\text{bottom}}$  as found above for  $D_{\text{shear}}$ . The sum of  $D_{\text{bottom}}$  and  $D_{\text{shear}}$  is then about  $10^{-7}$  W  $\text{kg}^{-1}$ , which is lower than but on the same order as the wave dissipation  $D$  computed above.

#### 4. Discussion

Additional two-layer KdV parameters for a system with layer thicknesses  $h_1$  and  $h_2$  and densities  $\rho_1$  and  $\rho_2$ , respectively, separated by an interface  $\zeta$  described by Eq. (1) are (Small 2001; Holloway 1987; Gear and Grimshaw 1983),

$$C_0^2 = \frac{g'h_1h_2}{h_1+h_2}; \quad g' = g\frac{\Delta\rho}{\rho_2}, \quad (5)$$

$$C = C_0\left(1 + \frac{ah_1-h_2}{2h_1h_2}\right), \quad \text{and} \quad (6)$$

$$L^2 = \frac{4}{3}\frac{h_1^2h_2^2}{(h_1-h_2)a}, \quad (7)$$

where  $a$  is negative for solitons of depression with  $h_1 < h_2$ . Upper- and lower-layer horizontal velocities are

$$U_1 = \frac{C_0\zeta}{h_1} \quad \text{and} \quad U_2 = -\frac{C_0\zeta}{h_2}, \quad (8)$$

with amplitudes  $b_{U1} = C_0a/h_1$  and  $b_{U2} = -C_0a/h_2$ , respectively.

Based on the layer parameters (top four rows of Table 3) and the fitted values of  $a_w$  (row 5), the quantities expressed in Eqs. (5)–(8) were calculated and are listed in Table 3 (rows 11–17). Note that that magnitude of  $C$  is about 10% greater than that of  $C_0$  for the four locations, reflecting the nonlinear contribution (6) to  $C$ . Also, the values of  $C$  in Table 3 are essentially the same as the mean value ( $0.51 \text{ m s}^{-1}$ ) found in section 3a, for the observations, and do not change significantly for the four locations. The amplitudes  $b_{U1}$  and  $b_{U2}$  are plotted in Fig. 14c (triangles) for comparison with observational values: these show quite good agreement and, except for  $U_2$  at A4, fall within the observed variability. There is generally a slight increase in horizontal velocity amplitude with increasing water depth, as was found for the observed values, but this may not be significant. These calculations [(5)–(8)] are dependent on stratification, and the CTD station associated with A4 was displaced about 2 km northeast and conducted 5 days later. There was some evidence of a front in the region, which may add uncertainty to the results.

The energy per unit crest length of a two-layer soliton is given by (Holloway 1987; Osborne and Burch 1980)

$$E = \frac{4}{3}\Delta\rho ga^2 L. \quad (9)$$

Calculated values of  $E$  appear in Table 3 for the four locations. The  $E$  values are comparable to those calculated directly from the data  $E_\zeta$  and show a similar decrease as the solitons move into shallower water.

#### 5. Conclusions

Six cases of strong NLIWs were identified on the outer continental shelf off New Jersey over a cruise period of about 10 days. The phase speeds were affected by the background currents, which were primarily tidally driven. Water depth and stratification also affected the overall characteristics of the waves. Advection-corrected phase speeds averaged  $0.51 \pm 0.09 \text{ m s}^{-1}$  along the mooring line. Uncorrected phase speeds differed from corrected phase speeds by 10%–20%. Average wavelength was about 300 m, and average wave period was about 10 min. Wave parameters were consistent between the various observational techniques that utilized both currents and hydrography. SeanFish tows at a fixed depth (see section 2) provided better wave characterizations than the profiling tows, because horizontal spatial aliasing could not be overcome by adjusting profiling parameters and ship speed. Wave amplitude decreased

in both vertical displacement and velocity with shallowing water depth. Wave energy correspondingly decreased as the waves propagated up the sloping bottom into shallower water. The observed internal solitons can be locally described by an inviscid, first-order, two-layer KdV model, but the apparent decrease in amplitude as the waves move into shallower water perhaps requires the use of a second-order (cubic) extended KdV or more a complex model to fully explain this decrease. On the other hand, frictional effects may be important in shallow water. Rough estimates of dissipation due to bottom drag and shear instabilities in the pycnocline are of the same order as the average dissipation inferred from the energy-flux divergence near the center of the mooring array.

*Acknowledgments.* The authors thank Justin Small for many helpful comments. This work was sponsored by the Office of Naval Research as part of the Naval Research Laboratory's "Forecasting Magnetic Fields Generated by Submesoscale Hydrodynamics" under program element 62435N.

#### REFERENCES

- Alford, M. H., R.-C. Lien, H. Simmons, J. Klymak, S. Ramp, Y. J. Yang, D. Tang, and M.-H. Chang, 2010: Speed and evolution of nonlinear internal waves transiting the South China Sea. *J. Phys. Oceanogr.*, **40**, 1338–1355.
- Colosi, J. A., R. C. Beardsley, J. F. Lynch, G. Gawarkiewize, C.-S. Chiu, and A. Scotti, 2001: Observations of nonlinear internal waves on the outer New England continental shelf during the summer Shelfbreak Primer study. *J. Geophys. Res.*, **106** (C5), 9587–9601.
- Dewey, R. K., and W. R. Crawford, 1988: Bottom stress estimates from vertical dissipation rate profiles on the continental shelf. *J. Phys. Oceanogr.*, **18**, 1167–1177.
- Djordjevic, V. D., and L. G. Redekopp, 1978: The fission and disintegration of internal solitary waves moving over two-dimensional topography. *J. Phys. Oceanogr.*, **8**, 1016–1024.
- Duda, T. F., J. F. Lynch, J. D. Irish, R. C. Beardsley, S. Ramp, C.-S. Chiu, T.-Y. Tang, and Y.-J. Yang, 2004: Internal tide and nonlinear internal wave behavior at the continental slope in the northern South China Sea. *IEEE J. Oceanic Eng.*, **29**, 1–27.
- Gear, J. A., and R. Grimshaw, 1983: A second-order theory for solitary waves in shallow fluids. *Phys. Fluids*, **26**, 14–29.
- Hallock, Z. R., and R. L. Field, 2005: Internal-wave energy fluxes on the New Jersey shelf. *J. Phys. Oceanogr.*, **35**, 3–12.
- Helfrich, K. R., and W. K. Melville, 2006: Long nonlinear internal waves. *Annu. Rev. Fluid Mech.*, **38**, 395–424.
- Holloway, P. E., 1987: Internal hydraulic jumps and solitons at a shelf break region on the Australian North West shelf. *J. Geophys. Res.*, **92** (C5), 5405–5416.
- Jackson, C. R., and J. R. Apel, cited 2004: An atlas of internal solitary-like waves and their properties. 2nd ed. Global Ocean Associates. [Available online at [http://www.internalwaveatlas.com/Atlas2\\_index.html](http://www.internalwaveatlas.com/Atlas2_index.html).]
- Johnson, G. C., R. G. Lueck, and T. B. Sanford, 1994: Stress on the Mediterranean outflow plume. Part II: Turbulent dissipation and shear measurements. *J. Phys. Oceanogr.*, **24**, 2084–2092.
- Klymak, J. M., and J. N. Moum, 2003: Internal solitary waves of elevation advancing on a shoaling shelf. *Geophys. Res. Lett.*, **30**, 2045. doi:10.1029/2003GL017706.
- , R. Pinkel, C.-T. Liu, A. K. Liu, and L. David, 2006: Prototypical solitons in the South China Sea. *Geophys. Res. Lett.*, **33**, L11607. doi:10.1029/2006GL025932.
- Large, W. G., J. C. McWilliams, and S. C. Doney, 1994: Oceanic vertical mixing: A review and a model with a nonlocal boundary layer parameterization. *Rev. Geophys.*, **32**, 363–403.
- MacKinnon, J. A., and M. C. Gregg, 2003: Shear and baroclinic energy flux on the summer New England shelf. *J. Phys. Oceanogr.*, **33**, 1462–1475.
- Moum, J. N., and J. D. Nash, 2008: Seafloor pressure measurements of nonlinear internal waves. *J. Phys. Oceanogr.*, **38**, 481–491.
- , J. M. Klymak, J. D. Nash, A. Perlin, and W. D. Smyth, 2007: Energy transport by nonlinear internal waves. *J. Phys. Oceanogr.*, **37**, 1968–1988.
- Osborn, T. R., 1980: Estimation of the local rate of vertical diffusion from dissipation measurements. *J. Phys. Oceanogr.*, **10**, 83–89.
- Osborne, A. R., and T. L. Burch, 1980: Internal solitons in the Andaman Sea. *Science*, **208**, 451–460.
- Perkins, H., F. De Strobel, and L. Gauldesi, 2000: The Barny Sentinel trawl-resistant ADCP bottom mount: Design, testing, and application. *IEEE J. Oceanic Eng.*, **25**, 430–436.
- Phillips, O. M., 1969: *The Dynamics of the Upper Ocean*. Cambridge University Press, 261 pp.
- Porter, D. L., and D. R. Thompson, 1999: Continental shelf parameters inferred from SAR internal wave observations. *J. Atmos. Oceanic Technol.*, **16**, 475–487.
- Shroyer, E. L., J. N. Moum, and J. D. Nash, 2008: Observations of polarity reversal in shoaling nonlinear internal waves. *J. Phys. Oceanogr.*, **38**, 691–701.
- , —, and —, 2010: Energy transformations and dissipation of nonlinear internal waves over New Jersey's continental shelf. *Nonlinear Processes Geophys.*, **17**, 345–360.
- Small, J., 2001: A nonlinear model of the shoaling and refraction of interfacial solitary waves in the ocean. Part I: Development of the model and investigations of the shoaling effect. *J. Phys. Oceanogr.*, **31**, 3163–3183.
- Sutton, O. G., 1953: *Micrometeorology*. McGraw-Hill, 333 pp.
- Tang, D., and Coauthors, 2007: Shallow Water '06: A joint acoustic propagation/nonlinear internal wave physics experiment. *Oceanography*, **20**, 156–167.
- Wijesekera, H. W., D. W. Wang, W. J. Teague, and E. Jarosz, 2010: High sea-floor stress induced by extreme hurricane waves. *Geophys. Res. Lett.*, **37**, L11604. doi:10.1029/2010GL043124.
- Zaron, E. D., and J. N. Moum, 2009: A new look at Richardson number mixing schemes for equatorial ocean modeling. *J. Phys. Oceanogr.*, **39**, 2652–2664.